Fusion Engineering and Design 194 (2023) 113731

Contents lists available at ScienceDirect

Fusion Engineering and Design

journal homepage: www.elsevier.com/locate/fusengdes

Front face shaping of the inner wall tiles in the COMPASS Upgrade tokamak

J. Gerardin [a], V. Balner [a], R. Dejarnac [a,*], M. Imrisek [a], F. Jaulmes [a], M. Komm [a], M. Peterka [a,b], P. Vondracek [a]

[a] Institute of Plasma Physics of the CAS, Za Slovankou 1782/3, Prague 8, 18200, Czech Republic
[b] Faculty of Mathematics and Physics, Charles University in Prague, Czech Republic

ARTICLE INFO

Keywords:
Plasma facing components
Field line tracing
Charged particles heat flux
Shaping
Shortwave misalignment

ABSTRACT

The central column of the COMPASS Upgrade tokamak, where the plasma discharges will be started and shut down, is covered by a continuous first wall composed of 8 bulk tungsten guard limiters with recessed Inconel tiles in between. In diverted configurations, the plasma will be limited for a short duration (~0.2 s–0.4 s) during the plasma current ramp-up and ramp-down phases but high heat fluxes due to short power decay lengths are foreseen. An adapted shaping is therefore needed to spread the heat loads over a maximum area. A novel method taking into account the different magnetic equilibria and the incident angle of the field lines was used to design a roof shape able to ensure a constant heat flux on the toroidal direction, accounting for the $\lambda_{qnear-SOL}$ and $\lambda_{qfar-SOL}$. Due to the diversity of plasma scenarios considered on COMPASS-U, the optimized shape of the inner wall tiles strongly differs from one scenario to another, thus a compromise has to be found among all foreseen scenarios. The tile shaping also needs to take into account possible short wave misalignments. Calculations with the 3D magnetic field line tracing code PFCFlux validates the design, confirming the constant toroidal profile of deposited heat flux for the COMPASS-U workhorse scenarios, or slightly decreasing or increasing heat flux profiles (from the center to the sides of the tile) for scenarios with smaller or higher $\lambda_{qnear-SOL}$, respectively, within the expected large range (1.7 mm< $\lambda_{qnear-SOL}$ <5 mm), but still providing acceptable loads. Estimated heat fluxes are in the range of 5 MW/m^2 to 35 MW/m^2 on the 8 guard limiters, receiving 70%–80% of the power deposited to the inner wall. In case of shortwave misalignments up to 0.5 mm in the radial direction, calculations show that leading edges are still protected, confirming the robustness of the design.

1. Introduction

COMPASS-Upgrade is a new medium size, high field tokamak (R = 0.9 m, a = 0.27 m, B_t = 5T, I_p = 2MA) currently under design in the Czech Republic, with metallic plasma facing components (PFC), the possibility to operate up to 500°C and heated by Neutral Beam Injection (NBI) and Electron-Cyclotron Resonance Heating (ECRH). It aims to address some of the key challenges in the field of power exhaust physics, advanced plasma configurations and confinement modes, new plasma facing materials and liquid metal divertor concepts [1,2].

The PFCs (Fig. 1) are inertial and cooled only by thermal diffusion to the structure, which limits the cooling of the PFCs during operations. The front face shape of the PFCs will influence the charged particle heat flux received, in particular due to a modification of the wetted area. It has not really influence on the radiative heat flux received. Thus, the front face shape has to be design in function of the charged particle heat flux, carried by the magnetic field lines. Due to the high parallel flux encountered inside fusion devices, the incident angle of the field line on the PFC should be maintained to a small value (1°–4°) and the design should take into account possible misalignment during the assembly of the PFCs. The current design of the plasma facing components is illustrated on Fig. 1, with a closed divertor on the bottom (made of Tungsten) and an open divertor on the top (made of Inconel).

In order to not reach critical temperature on the PFCs (below 2000°C for tungsten tiles and below 1000°C for Inconel tiles), the front face of the PFCs will be shaped in order to minimize the charged particles heat flux by keeping it uniform on the largest possible area for the different foreseen scenarios. It is also necessary to ensure that the leading edges are protected against high heat fluxes (the incident angle of the field line is close to 90° on the leading edges, resulting to a heat flux up to 20 times higher to the one on the top surface), meaning that the maximum heat flux should not be located on a leading edge. It does not mean that the leading edges have to be shadowed in any case, because far of the Last Closed Flux Surface (LCFS), the parallel heat flux carried by the magnetic field lines become so small that wetting the

* Corresponding author.
E-mail address: dejarnac@ipp.cas.cz (R. Dejarnac).

https://doi.org/10.1016/j.fusengdes.2023.113731
Received 27 October 2022; Received in revised form 9 March 2023; Accepted 4 April 2023
Available online 13 April 2023

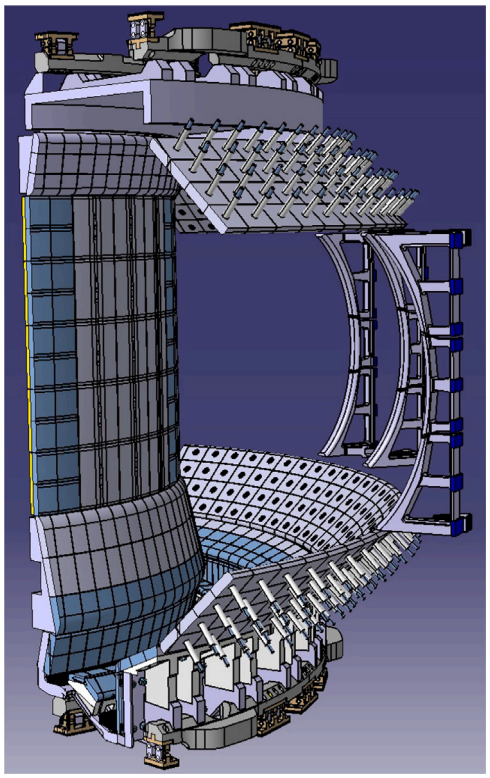

Fig. 1. 3D CAD view of the COMPASS-U metallic plasma facing components. Tiles are either made of bulk W (dark blue) or Inconel 718 (light gray), with the latter being coated by a thin layer of W.

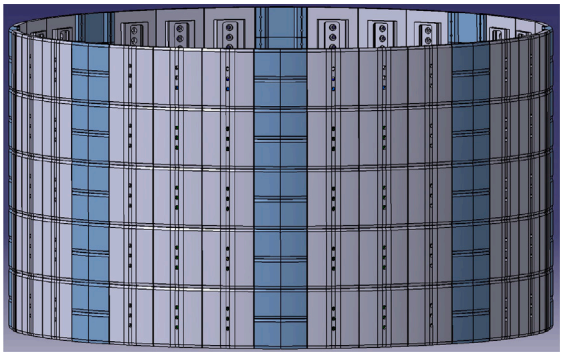

Fig. 2. Inner wall of COMPASS Upgrade. 8 columns of Tungsten tiles (dark blue) distributed every 45°. Other tiles made of Inconel 718 (light gray) with Tungsten coating.

leading edge with normal incidence does not create higher heat fluxes compared to the touching point area. Thus, far of the LCFS, there is no need to shadow the leading edges.

2. Design of the inner wall in COMPASS upgrade

This work is focused on the design of the inner wall in COMPASS Upgrade. The Fig. 2 shows the inner wall design. It is composed of 24 columns of Inconel tiles and 8 Tungsten guard limiters (distributed every 45°) which protrude towards plasma with respect to the Inconel tiles by 2 mm. The latter will collect a larger part of the heat flux during plasma current Ramp-Up (RU) and Ramp-Down (RD) phases.

Indeed, during RU and RD, the plasma will be located on the inner wall, involving several tens of MW/m^2 on the inner wall during up to 0.2–0.4 s. During the initial phase of COMPASS Upgrade, the plasma

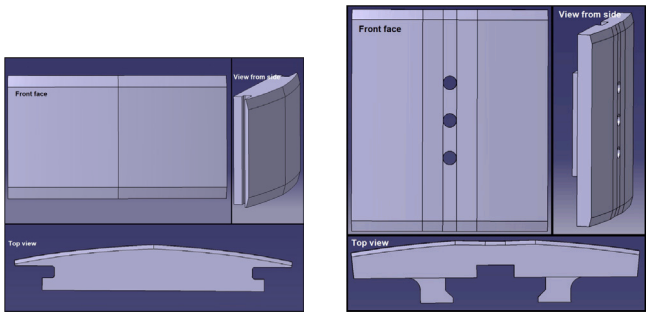

(a) Tungsten guard limiter tile. (b) Inconel tile.

Fig. 3. The two types of tiles composing the COMPASS-U inner wall.

scenarios will be mostly inner-wall limited, up to Bt = 5T and Ip = 1MA. It is thus of importance to optimize the shape of the inner wall PFCs to reduce the heat flux during these scenarios, which correspond to normal operating conditions. No off-normal events were taken into account for the design of these PFCs since it is the inner wall, so it will not be affected by ELM during H-mode (the heat flux is going only on the lower divertor) neither affected by VDEs (the plasma will hit the upper/lower baffle and stay enough far of the inner wall). Additional studies could be made in the future to study a loss of control of the plasma during a H-L transition, where the plasma could hit the inner wall.

2.1. Tungsten guard limiters

The major part of the heat flux will be deposited on 8 Tungsten guard limiters (WGL) (equally distributed every 45°, see Fig. 2). Each guard limiter is composed of 10 Tungsten tiles of 65 mm height and 115 mm width (see Fig. 3(a)). Pair of tiles are attached on a back plate, with a toroidal gap of 0.5 mm between the two tiles and separated with other pair of tungsten tiles by a toroidal gap of 1.5 mm. Each pair of tungsten tiles are separated toroidally with the surrounding Inconel tiles by a poloidal gap of 1.5 mm as well. A chamfer of 15° over 6 mm is made on horizontal top and bottom edges.

2.2. Inconel tiles

The remaining part of the inner wall is made on Inconel 718 tiles with a thin Tungsten coating. Each tile is of 130.5 mm height and 115 mm width, with a central attachment using three bolts on the front face for easy removal (see Fig. 3(b)), which will need a dedicated design to protect the holes (a double roof with two apexes, see Section 4). Poloidal and toroidal gaps with neighboring tiles are 1.5 mm wide. As for the WGL, chamfer of 15° over 6 mm is made on horizontal top and bottom edges.

3. Field line tracing calculations

3.1. PFCFlux

Charged particles heat flux calculation using 3D field line tracing codes are widely used to estimate the heat load on PFCs for different plasma configuration. SMARDDA [3] (included inside SMITER [4]) was used to estimate the charged particle heat flux on DEMO first wall and limiter with some misalignments [5,6] or used on JET divertor for thermo-mechanical modeling [7]. PFCFlux was used on WEST [8], JET [9], ITER [10], DEMO [11], EAST [12], CFETR [13]. Integrated tool containing a field line tracer module HEAT was used on NSTX-U [14].

The 3D field line tracing code used for this study was PFCFlux. The charged particles heat fluxes on the inner wall tiles during RU and RD

phases will be estimated. The main assumptions of PFCFlux are that particles come from the Outer Mid Plane (OMP) and will strictly follow the magnetic field lines. A parallel heat flux function (defined by the user, it can be for example an exponential decay) is set at the OMP and is then mapped to the PFCs in function of the magnetic flux of the scenario. The calculation of the magnetic shadowing is made in backward direction (from the PFC to the OMP). A PFC will receive heat fluxes from the plasma if it is magnetically connected to the OMP.

For limited plasma, the heat flux function which defines the parallel heat flux in the Scrape-Off Layer (SOL) from the OMP is made with two exponential decay, following the expression [10]:

$$q_{\parallel}(d) = q_{\parallel}(0,n) \times \left(e^{\frac{-d}{\lambda_{q_n}}} + \frac{1}{R_q} e^{\frac{-d}{\lambda_{q_f}}} \right) \quad (1)$$

where λ_{q_n} relates to the near-SOL decay length while λ_{q_f} is for the far-SOL decay length, $q_{\parallel}(0,n)$ is the parallel flux at the Last Closed Flux Surface (LCFS), d is the distance to the LCFS. R_q describes the ratio between near-SOL and far-SOL parallel heat flux:

$$R_q \equiv q_{\parallel(0,n)} / q_{\parallel(0,f)} \quad (2)$$

The heat flux on the target q_t is given by

$$q_t = q_{\parallel} \times \frac{R_{OMP}}{R} \times sin(\alpha) \quad (3)$$

where $q_{\parallel}$ is the parallel heat flux carried by the magnetic field line (from Eq. (1)), $\frac{R_{OMP}}{R}$ is the magnetic expansion and α is the incident angle of the field line on the PFC.

3.2. Studied scenarios

COMPASS Upgrade will aim to study various different plasma scenarios, from limited plasma to various Lower Single Null (LSN) or Upper Single Null (USN) configuration, heated by up to 4 MW of NBI and 2 MW of ECRH.

The scenarios are designed with the use of METIS [15]. It requires as input information about the shape of the plasma and the scenario wanted (R, a, B, I_p, κ). It also need the mean density, Z_{eff} and the composition of the plasma to calculate the radiative losses. Associated with a scenario of heating power (injected power from NBI and ECRH), METIS is able to calculate the ohmic power, the effective plasma heating of ions and electrons and the radiative power losses on the electrons. An estimation of the power inside the SOL (P_{SOL}) is made in function of the injected power, ohmic power, radiative losses and dW/dt.

The magnetic equilibria at each timestep of the scenario are simulated by FIESTA [16].

To estimate the near-SOL decay length λ_{q_n}, a scaling from [17] was used:

$$\lambda_{q_n} = 5671 \times {P_{SOL}}^{1/8} \frac{(1+\kappa^2)^{5/8} a^{17/8} B^{1/4}}{{I_p}^{9/8} R} \times \left(\frac{2\bar{A}}{1+\bar{Z}} \right)^{7/16} \left(\frac{Z_{eff}+4}{5} \right)^{1/8} \quad (4)$$

where κ is the plasma separatrix elongation, a the plasma minor radius, B the value of the vacuum toroidal field at the position of plasma major radius central position, I_p the plasma current, R the plasma major radius central position, Z_{eff} the plasma effective charge with alpha particles, assuming $\bar{Z} = 1$ and $\bar{A} = 2$ [17].

The far-SOL decay length λ_{q_f} comes from a mean of various scaling from [18].

The Table 1 gives a list of scenarios planned on COMPASS-Upgrade, among purely limited, LSN, or Negative Triangularity (NT) cases, yielding the largest scatter in λ_q during RU and RD. These scenarios were chosen in function of their diversity (very different parameters) or importance (scenario #5400 will be the main LSN scenario). As the design will not changed when the scenario will be different, it is important to ensure that a different scenario will not endanger the PFCs. Time evolution of plasma current I_p, total plasma energy W and power loss by the plasma P_{LOSS} are given on Fig. 4 for the different scenarios. The solid line correspond to the limited phase while dash line is during the diverted phase. The plasma current (Fig. 4(a)) RU and RD phases are mostly done during the diverted phase, the plasma is limited only during the beginning of the RU or the end of the RD. The plasma energy (Fig. 4(b)) remains below 80kJ during the limited phase, but the power loss by the plasma (corresponding to the power of the SOL) (Fig. 4(c)) can reach 4 MW during the NT scenario or 2 MW during the limited scenario #1401 which could create some high heat load on the inner wall. The Table 2 gives the estimated λ_{q_n}, λ_{q_f} and P_{SOL} during phases where the plasma is located on the inner wall (e.g. limited phase during RU and RD). The range of expected decay length are quite large (with a factor of 2.9 between smallest and largest λ_{q_n} and a factor of 1.9 for λ_{q_f}).

Table 1
Parameters of some of the foreseen plasma scenarios in COMPASS-U yielding the largest scatter in λ_q.

Scenario	B_T [T]	I_p [MA]	q_{95}	$\bar{n}_e$ [10^{20}m^{-3}]	$P_{NBI} + P_{EC}$ [MW]	Type of scenario
#1401	5	1	4.3	0.8	0+0	Lim.
#3100	2.5	0.8	3.2	1.2	0+0	LSN
#5400	5	1.6	3.6	2.2	4+2	LSN
#6403	5	2.0	2.7	2.3	4+2	LSN
#11300	2.5	0.5	3.9	0.9	2.8+1	NT
#13400	5	0.8	7.7	1.3	4+2	LSN

Table 2
Expected power decay lengths and P_{SOL} at an arbitrary time during each phase for the selected scenarios.

Scenario	λ_{q_n} [mm]	λ_{q_f} [mm]	P_{SOL} [MW]
#1401 FT	1.70	13.5	0.80
#3100 RU	2.70	12	1.08
#5400 RD	2.45	17.2	0.63
#6403 RU	4.89	13.5	1.06
#6403 RD	2.07	13.6	1.25
#11300 FT	4.10	9.0	4.03
#13400 RD	3.34	11.2	1.85

It is possible to optimize the shaping of the PFC for one particular power decay but for a wide range of power decay, the best compromise between all scenarios needs to be found. In function of the parallel heat flux decay length and flux expansion of the scenarios, the optimized shape can be more rounded or more straight (Fig. 5).

The magnetic equilibria corresponding to the scenarios in Table 1 are presented in Fig. 6, with the radial and vertical positions in meter for abscissa and ordinate. The mid plane is at z = 0 m.

4. Method to optimize the shape of the PFCs front face

An optimized shaping of the front face means that the heat flux is well distributed on the tile, at least toroidally, with the largest possible area wetted by the plasma to limit the maximum heat flux. The shaping needs also to shadow the leading edges of the neighboring component to avoid high heat fluxes due to almost normal incident angle. Thus, an axi-symmetric wall is not possible to use since the leading edges would be exposed. During RU and RD, on inner wall, the particles can hit the wall from both sides, it thus needs a roof-like symmetric shape.

Analytical methods were developed to obtain the optimized shape for a defined λ_q on a target, with a defined power decay law, like [10, 19,20] for the design of the inner wall of ITER. These methods rely on calculating a logarithmic shape which will compensate the exponential decay of power. This method will allow to obtain the exact shape needed for a particular λ_q and particular expression of the power decay, with one λ_q or two λ_q (λ_{qnear} λ_{qfar}). However, this analytical method

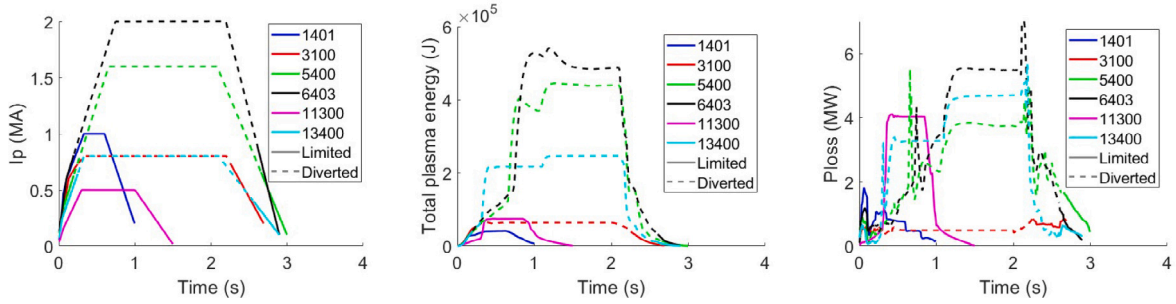

(a) Plasma current (MA). (b) Plasma total energy (J). (c) Plasma loss of power (MW).

Fig. 4. Time evolution of some plasma parameters for the different scenarios.

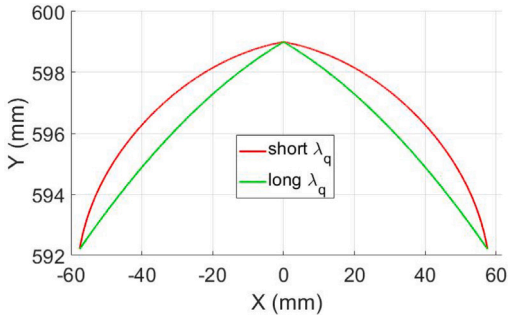

Fig. 5. Example of triangular shape for short and long decay length.

works only for this particular expression of power decay and to obtain the ideal shape for another expression of power decay, a new analytical expression has to be found.

A new way to obtain the exact shape needed to obtain a toroidally constant heat flux on the front face of a PFC is proposed, based on a numerical computation of the shape step by step. This method presents the advantage to be usable for any power decay expression.

4.1. Set back needed to protect the neighboring edges

The first challenge is to avoid leading edges, even in case of some possible misalignment of PFCs. Thus, the shape of the PFC needs to be adjusted so that the field line passing just above a PFC at grazing angle will not hit the side of the neighboring PFC at near normal incidence. The set back needed between the side of the PFC and the apex is function of the magnetic field of the scenario. The Fig. 7 shows the magnetic field lines passing above both apexes of the Inconel tiles and which will impact the central part of the inconel tile or the WGL. The magnetic field lines have not got the same inclination in function of their vertical position. For field line above or below the strike point, the radial magnetic field increase while the vertical magnetic field decreases, involving a more vertical inclination on the field line when you go far of the touching point vertical position. The different magnetic field line plotted here are for different parallel heat flux values. The far the field line is of the touching point and the smaller the parallel heat flux is due to the power decay. The magnetic field lines are represented for a parallel heat flux down to 5% of the parallel heat flux at the touching point. This value was chosen because when a leading edge is wetted, the heat flux will be approximatively 20 times higher, due to the increase of the sinus of incident angle (sin(87°)/sin(3°) = 19.1). So if any of these field line is wetting the leading edge, the maximum heat flux will be located on the leading edge. For all other field line further of the LCFS, so with a parallel heat flux less than 5% of the parallel heat flux at LCFS, if they wet the leading edge, they will not increase the maximum heat flux compared to the LCFS one on the front face. These field lines will not be critical for the design and shadowing the leading edges is thus not mandatory in all cases.

On Fig. 8, the magnetic field line presenting the highest needed set back (for a relevant parallel heat flux, as defined above) for each scenario is extracted. For the majority of the scenarios, the needed set back is at around 3 mm for the WGL and 1 mm for Inconel tiles. For the negative triangularity scenario (#11300), the set back needed is of 3.6 mm for the WGL and 1.6 mm for the Inconel tiles. A margin is added to allow some tolerance of shortwave misalignment (misalignment of a PFC with the neighboring one). Thus, set back of 2 mm for the Inconel tiles and 4 mm for the Tungsten limiter were chosen. This allows almost a misalignment of 0.5 mm for the negative triangularity scenarios (which are not the main scenarios) and 1 mm of misalignment for the large majority of the scenarios. For the central part of the inconel tiles, with a shaping needed to protect the holes for the bolts, a set back of 0.5 mm is needed for the majority of the scenarios. For the NT scenario, some field lines have a too large incident angle because of a too low toroidal magnetic field compared to the poloidal one and therefore the holes are not fully protected. However, these field lines are far from the LCFS, therefore not carrying the highest power. A higher set back on the central part (more than 0.5 mm) would lead to an increase of the incident angle of the field lines on the whole Inconel tiles and this would strongly increase the heat fluxes by reducing the wetted area for the large majority of the scenarios. As NT scenarios are not the main scenarios, if hot spots are detected (by Infrared camera systems) during the future experiments, the operation for such NT scenarios will be reduced, e.g., by lowering the power and/or the plasma duration.

4.2. How to get toroidally constant heat flux

The perpendicular heat flux (defined in Eq. (3)) aims to be constant on the tile to avoid gradients and as low as possible to minimize heating of the components. It is thus needed to determine how each term of this equation evolve with respect to the radial position. The $\frac{R_{OMP}}{R}$ ratio is modified by only 1%–2% in the range of radial position studied so its influence can be considered as negligible in the present study.

The parallel heat flux function defined at the OMP is function of the decay lengths λ_{q_n} and λ_{q_f}. On Fig. 9(a), different normalized parallel heat flux functions are represented for different distances to the LCFS and for the scenarios presented in Section 3.2. Due to the different decay lengths, some scenarios see their parallel heat flux decreasing more or less faster in the SOL. With the short λ_{q_n}, the parallel heat flux decreases by 60% to 80% in the first 5 mm after the LCFS. Different time slices of one scenario, e.g., scenarios #6403, can present large discrepancies of parallel heat flux decrease, since during the RU, the decay lengths are much larger than during the RD. Some scenarios can presents a relatively similar λ_{q_n} (e.g. scenario #3100 and #5400) and thus have a similar parallel heat flux decrease for a distance up to 6 mm to the LCFS at the OMP. But the different λ_{q_f} on these scenarios make then the parallel heat flux decrease different, with a smaller one for the scenario #5400 (larger λ_{q_f}).

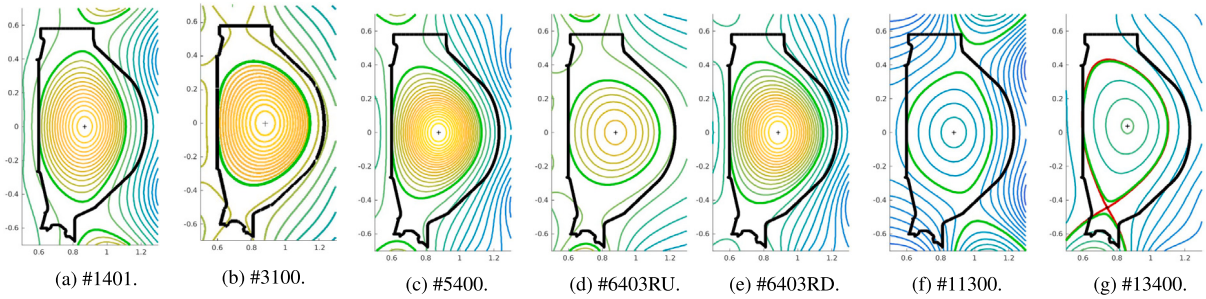

Fig. 6. Magnetic equilibria of the selected plasma scenarios.

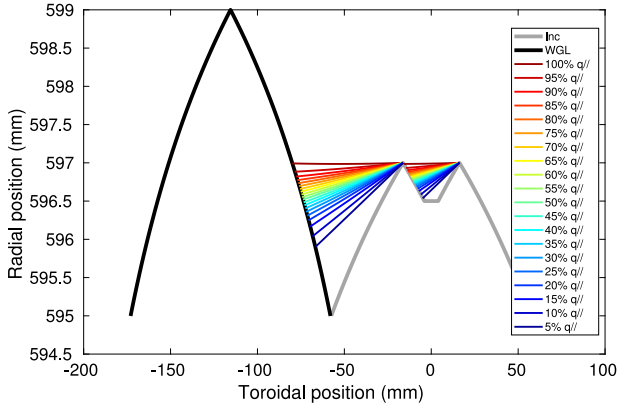

Fig. 7. Field lines passing by the two apexes of the Inconel tile (right) and interacting with the WGL tiles (left), coming from right to left, for the scenario 1401. The color correspond to the intensity of the field line, taken from different vertical positions.

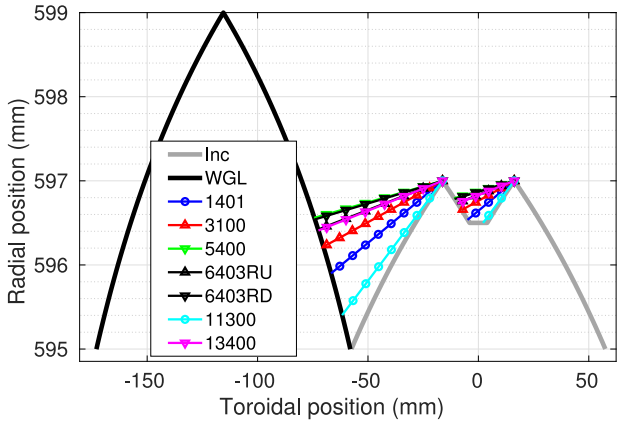

Fig. 8. Field lines passing by the two apexes of the Inconel tile (right) and interacting with the WGL tiles (left), coming from right to left, with the highest set back needed with at least 5% of the parallel heat flux, for the different scenario.

On Fig. 9(b), the distance to the LCFS at the OMP is represented for each scenario, for different radial positions on the target (at a fixed vertical position, here the touching point position on the target, at z = 6.75 mm). This figure expresses the radial magnetic compression of the field line. When a curve is above the dash gray line, it means that the field lines are more compressed on the OMP side. For the scenarios #6403 and #3100, a field line at a radial distance of 5 mm to the touching point will be at around 4 mm to the LCFS at the OMP, while for the scenarios #11300, this field line will be at only 2.5 mm to the LCFS, due to an higher compression of field line at the OMP.

By combining Figs. 9(a) and 9(b), one gets the normalized parallel flux as a function of the radial position on the target (see Fig. 9(c)). This highlights the fact that the flux expansion is an important parameter to take into account. Despite a narrower λ_{q_n} for the scenario #11300 compared to scenario #6403RU, its parallel heat flux decrease less on the target, due to a much stronger compression of the field line on the OMP. Scenarios #3100 and #5400 presents very similar parallel heat flux decreases, showing that for this range of radial positions on the target, the effect of the λ_{q_f} is not important.

Since the parallel heat flux on the target is decreasing with the radial position, an increase of the incident angle α of the field lines on the target can compensate this decrease of parallel heat flux (see Eq. (3)) to keep a constant heat flux. Thus, the optimal angle β on the PFC front face as function of its radial position can be deduced from Fig. 9(c) and is calculated from the needed incident angle α of the field lines to compensate the power decrease and from the incident angle α_{axisym} induced by the field line on an axisymmetric PFC (see Fig. 9(e) for the representation of the different angles), following:

$$\beta = \alpha - \alpha_{axisym} \tag{5}$$

The radial evolution of the angle β on the PFC to have a constant heat flux is shown on Fig. 9(d). Cases with higher decrease of power (like scenario #1401) will see their angle evolving from 2.2° to 9.1° while scenarios with smaller decrease of power (like scenario #11300) will see a less evolving angle between 3.1° to 5.7°.

The shape of the front face is then deduced step by step, starting from the apex. There is actually an infinity of possible shapes which allow a constant flux, depending on the initial angle β_1 defined at the apex. This angle has to be calculated so that the radial position at the side of the PFC gives the set back needed calculated on Section 4.1.

Starting from an initial angle defined at the apex β_1, a small toroidal step along the PFC tile is performed. A radial step is done to obtain the desired angle β_1. From this new radial position, the needed angle β_2 is deduced from Fig. 9(d). A new toroidal step is done, then a new radial step to obtain the angle β_2 etc. The procedure is repeated until the total toroidal extend of the PFC tile is reached (see Fig. 9(e)). If the obtained set back is too large, the initial angle is also too large and need to be reduced. On the contrary, if the set back obtained is too small, the initial angle at the apex has to be larger. A new calculation is performed with an adjusted angle to obtain a better set back and the process is repeated several times to finally get the wanted set back for the wanted toroidal extend. On Fig. 9(f), the different optimized shapes of the WGL for each scenario are plotted, from the apex to the side (the global PFC uses a symmetry of this shape to obtain a triangular shape like in Fig. 5). The initial angle at the apex shown on Fig. 9(d) are the one to obtain the wanted set back and are different for each scenario.

The shape for the scenario #3100 was chosen for the design of the WGL and Inconel tiles. This scenario corresponds to one main scenario for the first phase of the COMPASS-Upgrade operation, the optimized shape is also really close to the one of the scenario #5400, and this shape is a good balance between cases with shorter λ_{q_n} like #1401 or #6403RD and cases with longer λ_{q_n} like #11300 and #6403RU. With this shape, the heat fluxes will be slightly more concentrated close to

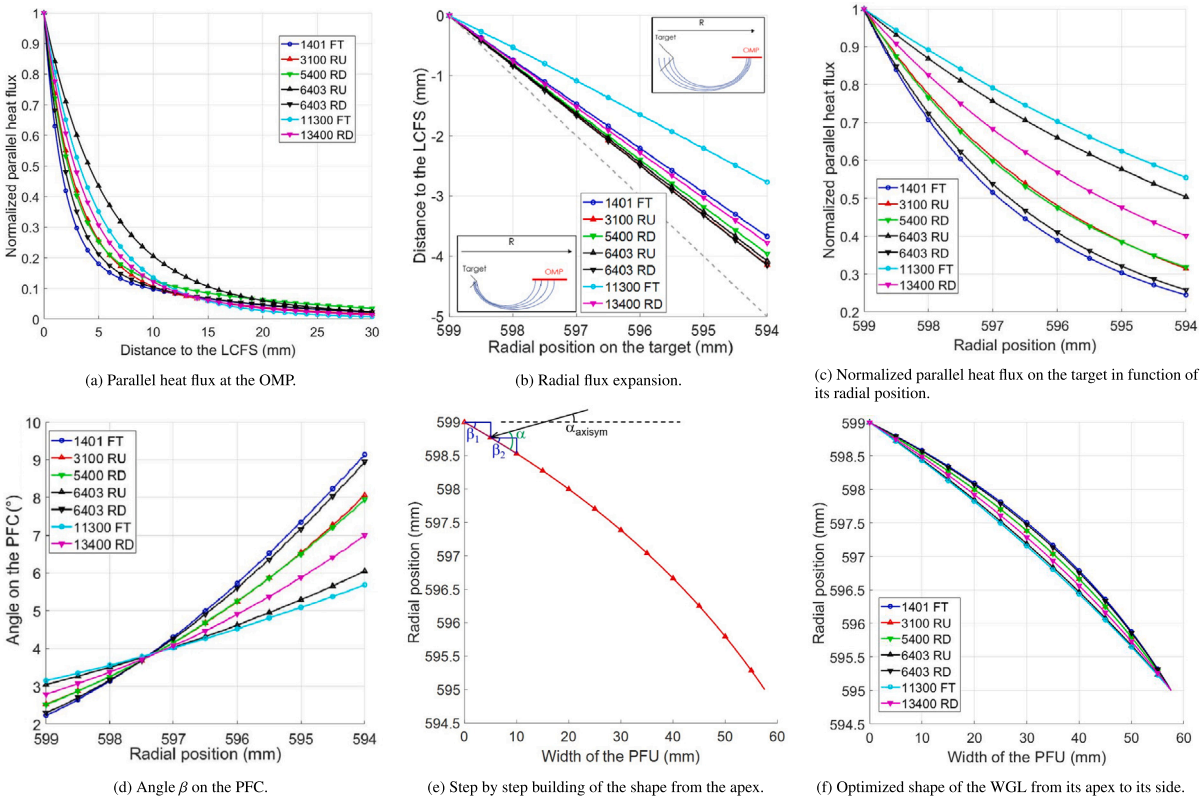

(a) Parallel heat flux at the OMP.

(b) Radial flux expansion.

(c) Normalized parallel heat flux on the target in function of its radial position.

(d) Angle β on the PFC.

(e) Step by step building of the shape from the apex.

(f) Optimized shape of the WGL from its apex to its side.

Fig. 9. Normalized parallel heat flux, flux expansion, angle on the PFC shape and corresponding optimized shape.

the apex for shorter λ_{q_n} cases and more on the side of the PFC for longer λ_{q_n}.

The shape of the Inconel tiles was calculated in the same process, keeping the touching point defined on the WGL. Thus, the normalized parallel heat flux in function of the radial position on the Inconel tiles still can be defined by the curves on Fig. 9(c), but from the radial position R = 597 mm. This part of curve were rescaled to have a maximum normalized parallel heat flux at 1 for R = 597 mm and then used in the same previous process to define the angle on the Inconel tiles and thus the optimized shape for any scenarios. The shapes on the central parts are symmetric to the shapes on side parts.

5. Result of heat flux loading on the optimized shape

5.1. Aligned cases

For these first studies, results on perfectly aligned PFC will be presented. Meshes of the WGL and Inconel tiles were made with a mesh size varying between 1 mm to 5 mm, to keep a discrepancy between the CAD model and the mesh (due to the curvature of the shape) below than 0.1 mm. An automatic refinement of the mesh was also made at the boundary between area wetted by the plasma and the ones magnetically shadowed, reducing the mesh size down to around 0.1 mm at these boundaries.

5.1.1. Spatial evolution of heat flux profiles for scenario #3100

The first result will be on the scenario #3100RU for which the shape was optimized (Fig. 10). All colored areas correspond to the inner wall wetted by the plasma, while all blank areas are magnetically shadowed. The heat flux is mainly concentrated on the WGL with a maximum heat flux of 13.4 MW/m2 while the maximum heat flux on inconel tiles is of 4.4 MW/m2 (see Fig. 10(a)). On the WGL where the maximum heat flux is located, three different horizontal profiles were drawn at different vertical positions (10 mm above or below the poloidal chamfer and at half height, see Fig. 10(b)). This WGL is located just above the mid plane (the midplane is at z = 0 mm while the bottom side of this WGL tile is at z = 0.75 mm). In this region above midplane, the field lines are going from right to left in the standard configuration (forward fields in clockwise direction from top), but some field lines are able to wet the bottom left part of this WGL tile coming from the region below the mid plane, from left to right. On Fig. 10(c), one can see the charged particles heat flux on each of these profiles on the WGL. The heat flux is toroidally constant for each profile, even if they have different magnitudes between left and right side, since different magnetic field lines are impacting the same vertical position of the PFC. The magnitude are also decreasing from bottom to top part of the tile, since the touching point is located on the bottom. The top part of the WGL is thus further away of the LCFS.

5.1.2. Time evolution of heat flux profiles for scenario #6403

The heat flux profile along the toroidal bottom slice of the WGL (see Fig. 10(b) for the location of the slice) is plotted for different time of the scenario #6403 on Fig. 11. During this scenario, the λ_{q_n} is evolving by a factor 2.4 between the shortest and the largest values (see Table 3). The heat flux profiles for these different time slices cannot be toroidally constant due to this strong variation of λ_{q_n}. For the time slices at t = 0.05 s or at t = 2.85 s, when the λ_{q_n} is the largest, the heat flux profile is increasing toroidally from the apex to the side (blue triangle up and black triangle down), while the profile is slightly decreasing from the apex to the side at t = 2.60 s when λ_{q_n} is minimal (blue triangle down). In general, the profile is relatively toroidally constant for most of the time slices. Optimizing the shape of the WGL for the time slice at t = 0.05 s would reduce the maximum heat flux only from 21 MW/m2 to 19.5 MW/m2 by making it toroidally constant, whilst creating toroidal heat flux gradients for most of the other time slices, what is preferable to avoid.

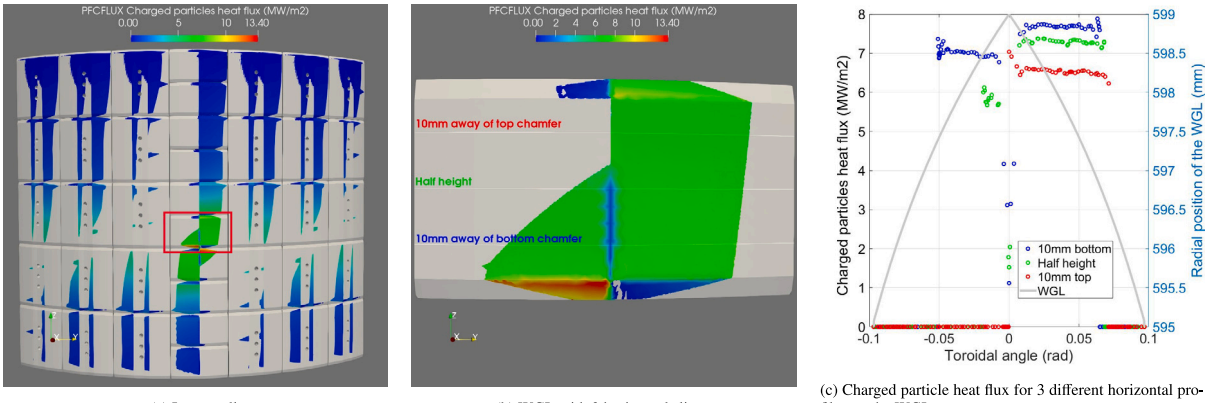

(a) Inner wall.

(b) WGL with 3 horizontal slices.

(c) Charged particle heat flux for 3 different horizontal profiles on the WGL.

Fig. 10. Charged particle heat flux during ramp-up of scenario #3100.

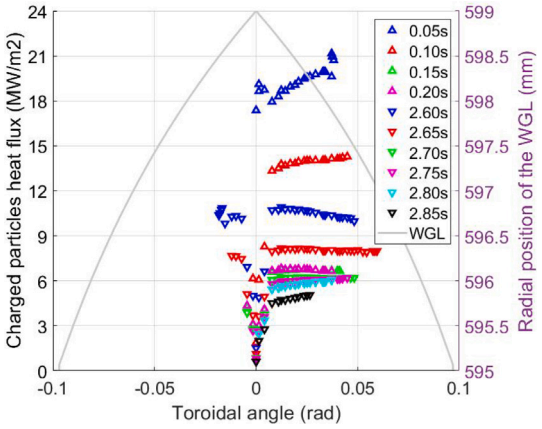

Fig. 11. Toroidal profiles of the charged particles heat flux on the WGL for different time slices of scenario #6403.

Table 3
Expected decay lengths and P_{SOL} at different time slices of scenario #6403.

Time slice [s]	λ_{q_n} [mm]	λ_{q_f} [mm]	P_{SOL} [MW]
0.05	4.89	13.5	1.06
0.10	3.19	14.1	1.00
0.15	2.57	16.8	0.59
0.20	2.34	15.6	0.64
2.60	2.07	13.6	1.25
2.65	2.30	15.9	0.95
2.70	2.44	17.2	0.64
2.75	2.77	17.2	0.53
2.80	3.41	17.6	0.42
2.85	4.87	19.2	0.30

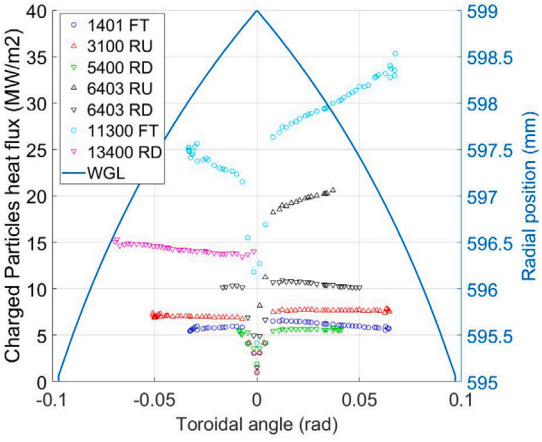

Fig. 12. Toroidal profiles of the charged particles heat flux on the WGL for different scenarios.

5.1.3. Comparison of heat flux profiles for all scenarios

A comparison of toroidal profiles extracted from the bottom part of the WGL tile for different scenarios is shown on Fig. 12. At the apex, the heat fluxes are close to zero, since the incident angle is almost null. After few millimeters (due to the mesh size), the heat fluxes are at a relevant value. The profile of scenarios #3100 and #5400 are flat since the shape is well optimized for these scenarios. For some scenarios with slightly narrower decay length λ_{q_n} (#1401, #6403RD), the heat fluxes are higher on the central part of the WGL tile and decrease slightly towards its side. For scenarios with wider decay length λ_{q_n} (#6403RU, #11300, #13400), the heat fluxes are minimal at the central part of the WGL tile and increase towards its side. This highlights the compromises to be found for this shape. The negative triangularity scenario (#11300) is showing the biggest variation of heat flux between the central part and the side (globally from 26 MW/m2 close to the central part to 35 MW/m2 on the side). A better compromises could be chosen to limit this range of heat flux fluctuation, by using a shape for higher decay length (like the shape optimized for the scenario #13400), but as the NT scenarios represent only a very small fraction of COMPASS-Upgrade future scientific operation, it was decided to stay with the current shape, best optimized for the large majority of the scenarios. With the current shape, excluding scenario #11300, the maximum variation of heat flux between the central part and the side of the WGL tile is 2.4 MW/m2 for the RU of scenario #6403.

5.2. Shortwave misalignment

A shortwave misalignment represents a misalignment between a PFC and its neighboring one, leading to potential exposed leading edges.

A PFCFlux calculation with a radial misalignment of two WGL tiles, located around the mid plane (in red on Fig. 13(a)), was performed for the scenario #1401. The radial misalignment of 0.5 mm (see Fig. 13(b)) can expose the leading edges of these WGL tiles to particles impacting with a normal incidence and can create hot spots along this edge. It is mandatory to protect the leading edges for the misalignment. The present design made with a set back of 4 mm should be able to ensure a radial misalignment of 0.5 mm between two neighboring PFCs, without creating leading edges (see Fig. 7).

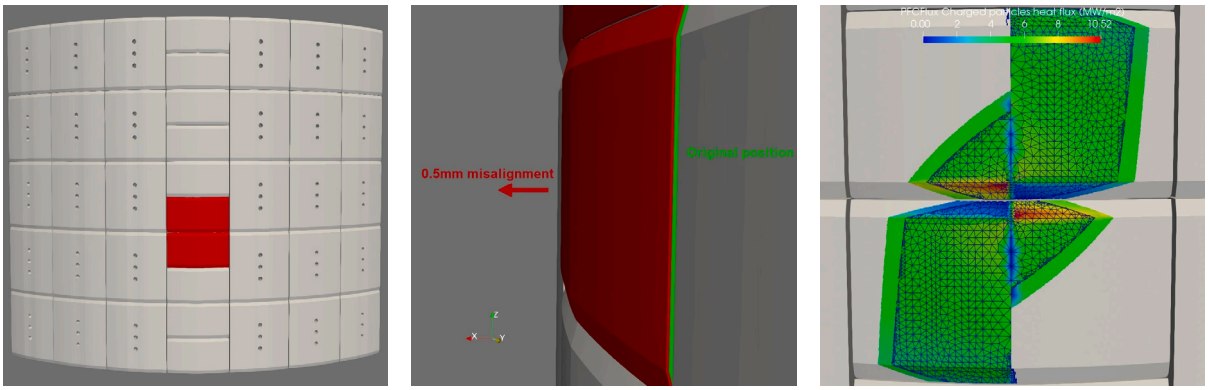

(a) Location of the misaligned guard limiters.

(b) Radial misalignment of the guard limiter by 0.5mm. The original position of the guard limiter is in green, the misaligned position in red.

(c) Comparison of the area wetted by the plasma between aligned PFCs (triangles) and misaligned PFCs (color), scenario #1401.

Fig. 13. Shortwave misalignment of two WGL tiles for scenario #1401.

The location of these WGL tiles is where the parallel heat flux is maximum, so where a wetted leading edge would cause the strongest heat fluxes.

The Fig. 13(c) highlights the difference of area wetted by the plasma during aligned and misaligned cases. The area with triangles corresponds to the surface wetted by the plasma with perfectly aligned PFCs, while the colored area is the one with the misalignment (and show the value of expected heat fluxes on this tile). The wetted area for the misaligned WGL tile is bigger since it is less shadowed by the neighboring PFCs. However, even if the PFC is misaligned, the leading edge is still protected by the neighboring PFCs. For this case, the misalignment is not enough significant to influence the heat flux pattern, almost similar heat fluxes are calculated on the tiles between the aligned and misaligned case.

5.3. Poloidal chamfer

A poloidal chamfer of 15° on 6 mm was added on top and bottom part of each WGL tiles and Inconel tiles. Without poloidal chamfer, high heat fluxes (above 100 MW/m^2) were observed on top or bottom part of some WGL tiles or Inconel tiles, due to the presence of the touching point around the horizontal gap between two tiles. Some magnetic field lines were able to reach these part of the tile (see Fig. 14). As these magnetic field lines impact the tiles with a large incident angle (around 14°) and can be very powerful (close to the LCFS), the resulting heat fluxes are high. As a consequence, the poloidal chamfer was added. It has two purposes. The first one is obviously to reduce the incident angle of the magnetic field line (see Fig. 15), where the incident angle can decrease from 14° (with no chamfer) to 10° with a chamfer of 45° and less than 4° for a chamfer of 15°. The second one is to put the bottom/top faces further of the LCFS, in order to reduce the heat fluxes they could receive with a large incident angle of field line.

The set back needed is tough to calculate in this case. Contrary to the estimation for the front face, where the radial position of the apex is constant vertically and the radial position on the neighboring tile is also constant vertically and making the calculation easy, for the poloidal chamfer, the radial position on both side are evolving toroidally since the chamfer is following the shape of the PFC. At the mid plane, the radial magnetic field is negligible, meaning that the radial position of the "apex" (green point) will hit the poloidal chamfer at a similar radial position on the neighboring tile (red point), but as this radial position is evolving toroidally, the set back needed will depend on each starting position. Moreover, when adding a larger chamfer, this increase the toroidal distance traveled by the field line flowing between both chamfer. Thus, the field line can pass just above the chamfer of one tile and reach the chamfer of 1 or 2 neighboring tiles further (so it can pass from an Inconel tile to a neighboring W tile or Inconel tile further). A trial and error method was used with different sizes and angles of poloidal chamfer with PFCFlux calculations to check if some high heat fluxes are still present on top/bottom part of the PFCs. The final chamfer chosen is of 15° which offer a decent incident angle of the magnetic field line (less than 4°) and a distance of 6 mm gives enough setback to collect the heat fluxes and put the top/bottom faces enough far of the LCFS to received eventually smaller heat fluxes than on front face. For the tiles around the midplane, the maximum heat fluxes will be still on the poloidal chamfer since it is the location of the touching point and the field line will impact the poloidal chamfer with a slightly higher incident angle compared to the front face.

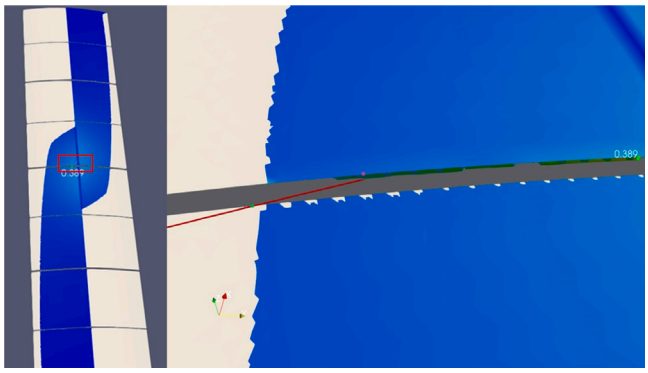

Fig. 14. Magnetic field line impacting the bottom part of a WGL tile, without poloidal chamfer. High heat fluxes are expected on a width of several hundreds of micrometers for this case.

6. Conclusion

COMPASS-Upgrade tokamak is under design, involving the need to design the metallic PFCs which will receive the charged particle heat loads from the plasma. The front face shape needs to be optimized in order to reduce the thermal stresses on the PFCs by having a constant heat flux and also needs to prevent hot spots (which could provoke melting and cracking) in case of misalignment of tiles.

A method to calculate an optimized shape of the inner wall of COMPASS-Upgrade in order to homogenize the heat flux on the PFC was established, in function of the power decay in the SOL and the flux expansion of the magnetic equilibrium. This method determines how the angle of the shape evolve toroidally so that the increase of the incident angle of the field lines on the PFC compensates the decrease of the parallel heat flux.

As the expected scenarios on COMPASS-Upgrade present a wide range of λ_q and flux expansion, the shape is optimized for only one scenario (and actually, at one time of the scenario). The shape chosen

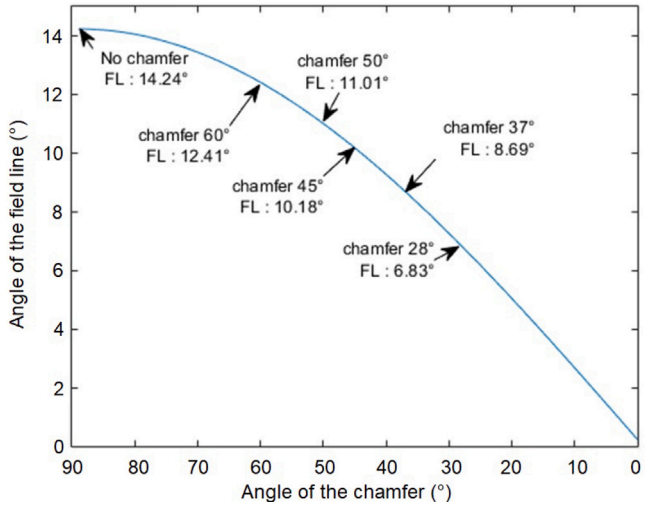

Fig. 15. Evolution on the incident angle of the magnetic field line on the chamfer in function of its angle.

need to offer a good compromise between scenarios with short λ_q and those with large λ_q.

3D field line tracing calculations were done with the code PFCFlux and confirm the toroidally constant heat flux on an optimized shape of PFCs. When scenarios present narrower λ_q than the optimized shape, the heat fluxes are decreasing linearly from the apex to the side of tiles and for larger λ_q, the maximum heat flux is on the side on the tile and decreasing toward the apex. The optimized shape chosen offers a good compromise among narrow λ_q and large λ_q and is convenient for most scenarios, especially when accounting for their time evolution. The shaping also offers a margin for the radial misalignment of tiles for at least 0.5 mm.

This method was applied on a power decay in the SOL with using a double exponential decay, but any other power decay can be modeled, following some exponential decay or coming from transport code like SOLPS or SolEdge2D, making this method more flexible compared to an analytical solution obtained for a given exponential decay function.

Declaration of competing interest

The authors declare that they have no known competing financial interests or personal relationships that could have appeared to influence the work reported in this paper.

Data availability

Data will be made available on request.

Acknowledgment

This work has been carried out within the framework of the project COMPASS-U: Tokamak for cutting-edge fusion research (No. CZ.02.1.01/0.0/0.0/16_019/0000768) and co-funded from European structural and investment funds.

References

[1] R. Panek, et al., Conceptual design of the COMPASS upgrade tokamak, Fusion Eng. Des. 123 (2017) 11–16, http://dx.doi.org/10.1016/j.fusengdes.2017.03.002.
[2] P. Vondracek, et al., Preliminary design of the COMPASS upgrade tokamak, Fusion Eng. Des. 169 (2021) 112490, http://dx.doi.org/10.1016/j.fusengdes.2021.112490.
[3] W. Arter, V. Riccardo, G. Fishpool, A CAD-based tool for calculating power deposition on tokamak plasma-facing components, IEEE Trans. Plasma Sci. 42 (7) (2014) 1932–1942, http://dx.doi.org/10.1109/TPS.2014.2320904.
[4] L. Kos, et al., SMITER: A field-line tracing environment for ITER, Fusion Eng. Des. 146 (2019) 1796–1800, http://dx.doi.org/10.1016/j.fusengdes.2019.03.037.
[5] Z. Vizvary, et al., DEMO first wall misalignment study, Fusion Eng. Des. 146 (2019) 2577–2580, http://dx.doi.org/10.1016/j.fusengdes.2019.04.046.
[6] M. Richiusa, et al., Bare and limiter DEMO single module segment concept first Wall misalignment study by 3D field line tracing, Fusion Eng. Des. 160 (2020) 111839, http://dx.doi.org/10.1016/j.fusengdes.2020.111839.
[7] D. Iglesias, et al., Advances in predictive thermo-mechanical modelling for the JET divertor experimental interpretation, improved protection, and reliable operation, in: 27th IAEA Fusion Energy Conference, 2018.
[8] M. Firdaouss, T. Batal, J. Bucalossi, P. Languille, E. Nardon, M. Richou, Heat flux depositions on the WEST divertor and first wall components, Fusion Eng. Des. 98–99 (2015) 1294–1298, http://dx.doi.org/10.1016/j.fusengdes.2014.12.024.
[9] M. Firdaouss, et al., Modelling of power deposition on the JET ITER like wall using the code PFCFlux, J. Nucl. Mater. 438 (2013) S536–S539, http://dx.doi.org/10.1016/j.jnucmat.2013.01.111.
[10] M. Kocan, et al., Impact of a narrow limiter SOL heat flux channel on the ITER first wall panel shaping, Nucl. Fusion 55 (2015) 033019, http://dx.doi.org/10.1088/0029-5515/55/3/033019.
[11] J. Gerardin, et al., Simplified heat load modeling for design of DEMO discrete limiter, Nucl. Mater. Energy 20 (2019) 100568, http://dx.doi.org/10.1016/j.nme.2019.01.002.
[12] B. Zhang, M. Firdaouss, X. Gong, A. Ekedahl, X. Peng, X. Zhang, Study of power load pattern on EAST divertor using PFCFlux code, Fusion Eng. Des. 107 (2016) 58–63, http://dx.doi.org/10.1016/j.fusengdes.2016.04.001.
[13] F. Nian, et al., Modelling of the complete heat flux deposition on the CFETR first wall with neon seeding, Plasma Phys. Control. Fusion 63 (9) (2021) 095004, http://dx.doi.org/10.1088/1361-6587/ac0a3d.
[14] T. Looby, et al., A software package for plasma-facing component analysis and design: The heat flux engineering analysis toolkit (HEAT), Fusion Sci. Technol. 78 (1) (2022) 10–27, http://dx.doi.org/10.1080/15361055.2021.1951532.
[15] J. Artaud, et al., Metis: a fast integrated tokamak modelling tool for scenario design, Nucl. Fusion 58 (10) (2018) 105001, http://dx.doi.org/10.1088/1741-4326/aad5b1.
[16] G. Cunningham, High performance plasma vertical position control system for upgraded MAST, Fusion Eng. Des. 88 (12) (2013) 3238–3247, http://dx.doi.org/10.1016/j.fusengdes.2013.10.001.
[17] R. Goldston, et al., Heuristic drift-based model of the power scrape-off width in low-gas-puff H-mode tokamaks, Nucl. Fusion 52 (2011) 013009, http://dx.doi.org/10.1088/0029-5515/52/1/013009.
[18] J. Horacek, et al., Multi-machine scaling of the main SOL parallel heat flux width in tokamak limiter plasmas, Plasma Phys. Control. Fusion 58 (7) (2016) 074005, http://dx.doi.org/10.1088/0741-3335/58/7/074005.
[19] P. Stangeby, Analytic expressions for shaping analysis of the ITER outer wall, Nucl. Fusion 51 (11) (2011) 103015, http://dx.doi.org/10.1088/0029-5515/51/10/103015.
[20] P. Stangeby, The strong effect of gaps on the required shaping of the ITER first wall, Nucl. Fusion 51 (11) (2011) 033008, http://dx.doi.org/10.1088/0029-5515/51/3/033008.